












RESEARCH ARTICLE | SEPTEMBER 04 2024

## Beyond the “spine of hydration”: Chiral SFG spectroscopy detects DNA first hydration shell and base pair structures



Special Collection: [Festschrift in honor of Yuen-Ron Shen](#)






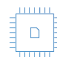
Ethan A. Perets ; Daniel Konstantinovsky ; Ty Santiago ; Pablo E. Videla ; Matthew Tremblay ; Luis Velarde ; Victor S. Batista ; Sharon Hammes-Schiffer  ; Elsa C. Y. Yan  



*J. Chem. Phys.* 161, 095104 (2024)


<https://doi.org/10.1063/5.0220479>



 Nanotechnology & Materials Science  Optics & Photonics  Impedance Analysis  Scanning Probe Microscopy  Sensors  Failure Analysis & Semiconductors

Unlock the Full Spectrum.  
From DC to 8.5 GHz.  
Your Application. Measured.

[Find out more](#)



# Beyond the “spine of hydration”: Chiral SFG spectroscopy detects DNA first hydration shell and base pair structures

Cite as: J. Chem. Phys. 161, 095104 (2024); doi: 10.1063/5.0220479

Submitted: 25 May 2024 • Accepted: 6 August 2024 •

Published Online: 4 September 2024



View Online



Export Citation



CrossMark

Ethan A. Perets,<sup>1,a)</sup>  Daniel Konstantinovsky,<sup>1,2,b)</sup>  Ty Santiago,<sup>1</sup>  Pablo E. Videla,<sup>1,c)</sup>  Matthew Tremblay,<sup>1</sup>  Luis Velarde,<sup>3</sup>  Victor S. Batista,<sup>1</sup>  Sharon Hammes-Schiffer,<sup>1,4,d)</sup>  and Elsa C. Y. Yan<sup>1,d)</sup> 

## AFFILIATIONS

<sup>1</sup> Department of Chemistry, Yale University, New Haven, Connecticut 06520, USA

<sup>2</sup> Department of Molecular Biophysics and Biochemistry, Yale University, New Haven, Connecticut 06520, USA

<sup>3</sup> Department of Chemistry, University at Buffalo, State University of New York, Buffalo, New York 14260, USA

<sup>4</sup> Department of Chemistry, Princeton University, Princeton, New Jersey 08544, USA

**Note:** This paper is part of the JCP Festschrift in honor of Yuen-Ron Shen.

<sup>a)</sup> **Current address:** Department of Molecular Biology, University of Texas Southwestern Medical Center, Dallas, TX 75390, USA.

<sup>b)</sup> **Current address:** Department of Chemistry, Columbia University, New York, NY 10027, USA.

<sup>c)</sup> **Current address:** Schrödinger, LLC, New York, NY 10036, USA.

<sup>d)</sup> **Authors to whom correspondence should be addressed:** [shs566@princeton.edu](mailto:shs566@princeton.edu) and [elsa.yan@yale.edu](mailto:elsa.yan@yale.edu)

## ABSTRACT

Experimental methods capable of selectively probing water at the DNA minor groove, major groove, and phosphate backbone are crucial for understanding how hydration influences DNA structure and function. Chiral-selective sum frequency generation spectroscopy (chiral SFG) is unique among vibrational spectroscopies because it can selectively probe water molecules that form chiral hydration structures around biomolecules. However, interpreting chiral SFG spectra is challenging since both water and the biomolecule can produce chiral SFG signals. Here, we combine experiment and computation to establish a theoretical framework for the rigorous interpretation of chiral SFG spectra of DNA. We demonstrate that chiral SFG detects the N–H stretch of DNA base pairs and the O–H stretch of water, exclusively probing water molecules in the DNA first hydration shell. Our analysis reveals that DNA transfers chirality to water molecules only within the first hydration shell, so they can be probed by chiral SFG spectroscopy. Beyond the first hydration shell, the electric field-induced water structure is symmetric and, therefore, precludes chiral SFG response. Furthermore, we find that chiral SFG can differentiate chiral subpopulations of first hydration shell water molecules at the minor groove, major groove, and phosphate backbone. Our findings challenge the scientific perspective dominant for more than 40 years that the minor groove “spine of hydration” is the only chiral water structure surrounding the DNA double helix. By identifying the molecular origins of the DNA chiral SFG spectrum, we lay a robust experimental and theoretical foundation for applying chiral SFG to explore the chemical and biological physics of DNA hydration.

Published under an exclusive license by AIP Publishing. <https://doi.org/10.1063/5.0220479>

## INTRODUCTION

Watson and Crick recognized that DNA secondary structure is a function of hydration content.<sup>1</sup> The “rather high” water content around DNA to which the scientists alluded was later elucidated by the discovery of a chiral helix of water molecules in the DNA minor groove.<sup>2–6</sup> This “spine of hydration” comprises ~2 water molecules per base pair<sup>3</sup> of double-stranded DNA (dsDNA) and accounts for

around 3%–6% of the first hydration shell.<sup>7</sup> Despite ample structural evidence for the spine of hydration, other water structures around dsDNA have eluded experimental characterization. Methods capable of probing dsDNA hydration structures beyond the spine of hydration promise a deeper understanding of how water influences dsDNA structure and determines the specificity of molecular binding and chemical reactivity. In this study, we combine experimental and theoretical approaches using chiral-selective vibrational

sum frequency generation (chiral SFG) spectroscopy and provide a rigorous interpretation of the chiral SFG spectrum of dsDNA hydration structures.

Vibrational spectroscopies, such as Raman,<sup>8,9</sup> ultrafast two-dimensional infrared (2DIR),<sup>10</sup> and terahertz spectroscopies,<sup>11</sup> offer sensitive, label-free approaches to probing hydration structures. Vibrational spectroscopies can distinguish dsDNA hydration shell water molecules by non-bulk-like water dynamics<sup>11–14</sup> or by distinct molecular interactions, for example, unique hydrogen-bonding structures compared to bulk water.<sup>15,16</sup> Alternatively, native molecular probes, such as the negatively charged phosphate groups of dsDNA, offer indirect readouts of hydration shell water structures and dynamics.<sup>10,17</sup> However, vibrational spectroscopies may fail to detect dsDNA hydration shell structures when the interactions or dynamics of water molecules in hydration shells are too similar to bulk water.

Recently, it has been recognized that chiral SFG can detect hydration structures around DNA and protein.<sup>6,18–22</sup> Chiral SFG is sensitive to the macroscopic chirality of biomacromolecules, such as protein secondary structures<sup>23–26</sup> and dsDNA<sup>27,28</sup> as well as chiral assemblies of achiral molecules.<sup>25,29–31</sup> Because water molecules are achiral, chiral SFG only detects chiral assemblies of multiple water molecules, such as the spine of hydration. Petersen and co-workers first reported chiral SFG vibrational signatures of O–H stretching of water around dsDNA.<sup>6</sup> They assigned the vibrational response to water molecules in the spine of hydration and attributed sequence-dependent effects in the chiral SFG spectra to sequence-dependent water structures within the dsDNA minor groove. Their pioneering study suggested that chiral SFG has high sensitivity and specificity for water molecules within the dsDNA hydration shell, which prompts two major questions. Can chiral SFG probe hydration structures beyond the minor groove spine of hydration, and detect water structures hydrating the major groove and phosphate backbone of DNA? What are the contributions of nucleotide vibrations in the chiral SFG response? Answering these questions is paramount for providing an accurate molecular interpretation of chiral SFG spectra of DNA.

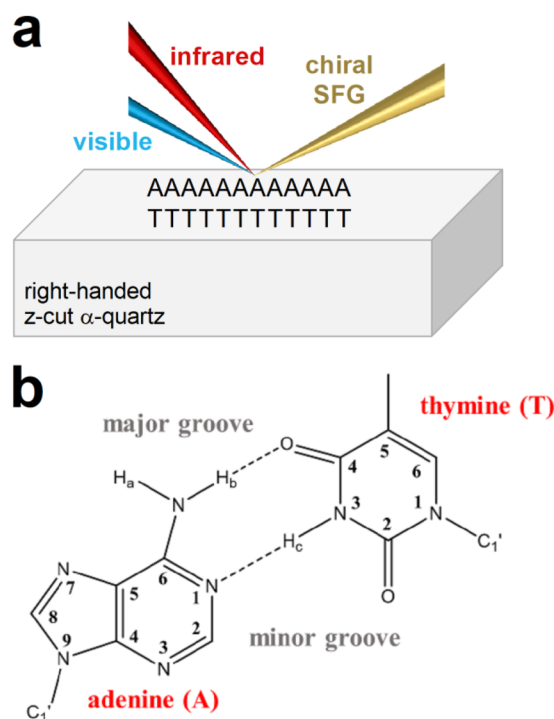
In this article, we address these two key questions using tandem experimental and computational chiral SFG approaches, akin to those developed in our previous studies of protein hydration.<sup>19,20,22,28,32,33</sup> We identify chiral SFG vibrational signatures from the O–H stretching of water molecules that form chiral hydration structures around  $(dA)_{12} \cdot (dT)_{12}$  dsDNA, as well as stretching modes of adenine  $NH_2$ , which forms hydrogen bonds in canonical adenine–thymine base pairs. Using native (D-) and non-native (L-) dsDNA enantiomers, we confirm that the handedness of the dsDNA double helix templates the handedness of chiral hydration structures around dsDNA. Overall, we demonstrate that N–H stretching of dsDNA, as well as O–H stretching of water molecules hydrating not only the minor groove but also the major groove and the phosphate backbone, can contribute to the chiral SFG response. Our results establish that chiral SFG is sensitive to dsDNA nucleotide vibrations as well as to hydration structures beyond the minor groove spine of hydration.<sup>6</sup> We conclude that chiral SFG is exclusively sensitive to the structure of the dsDNA first hydration shell. The ability of chiral SFG to study the structure of the first hydration shell around dsDNA will help answer important questions in DNA biology, including the role of water in DNA biomolecular

recognition, chromatin remodeling, epigenetic modification, and genetic regulation.

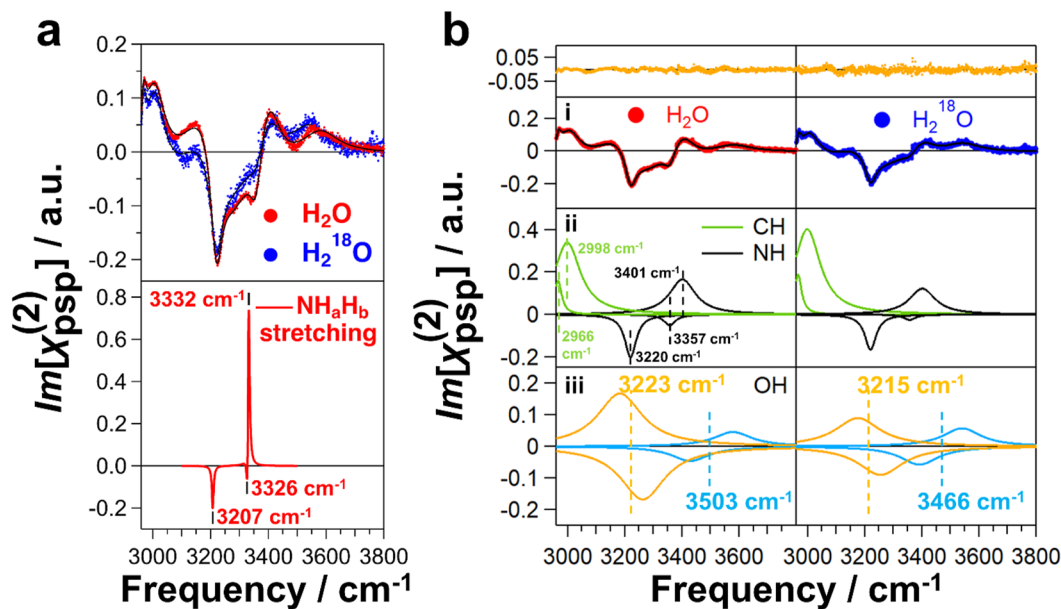
## RESULTS

### Chiral SFG reveals vibrational resonances due to water O–H and dsDNA N–H

We implement phase-resolved heterodyne chiral SFG for the study of dsDNA hydration (see Methods). In our experiments, hydrated films of  $(dA)_{12} \cdot (dT)_{12}$  dsDNA are dropcast on a right-handed z-cut  $\alpha$ -quartz crystal substrate under ambient conditions and probed by ultrafast pulsed infrared and visible lasers [Fig. 1(a)]. Overlapping the linearly polarized infrared and visible pulses in time and space at the sample surface enables detection of the chiral SFG response of water and dsDNA [Fig. 2(a), top]. We begin by assigning vibrational features in the experimental chiral SFG spectrum of  $(dA)_{12} \cdot (dT)_{12}$  dsDNA in the region of  $2960$ – $3800$   $cm^{-1}$ . Chiral SFG vibrations from  $2960$  to  $3100$   $cm^{-1}$  likely arise from C–H stretching modes of adenine, thymine, and/or the DNA sugar.<sup>28,34</sup> For  $(dA)_{12} \cdot (dT)_{12}$  dsDNA, vibrational resonances above  $3200$   $cm^{-1}$  can arise from adenine base  $NH_aH_b$  stretching [Fig. 1(b)] or water O–H stretching modes. Previous studies did not attribute N–H contribution in the chiral SFG spectra of  $(dAdT)_{12} \cdot (dAdT)_{12}$  dsDNA.<sup>6</sup> However, N–H and O–H vibrations can be experimentally



**FIG. 1.** (a) Schematic of chiral SFG spectroscopy of  $(dA)_{12} \cdot (dT)_{12}$  dsDNA hydrated films dropcast at the air-quartz interface. Chiral-sensitive *psp* polarization is achieved by detecting the *p*-polarized chiral SFG output with *s*-polarized visible and *p*-polarized infrared input laser beams (see Methods). (b) Adenine–thymine base pairs showing minor groove and major groove chemical moieties. Subscripts a, b, and c refer to positions of H atoms with unique H-bonding environments for discussion purposes.



**FIG. 2.** Experimental and calculated chiral SFG spectra of  $(dA)_{12} \cdot (dT)_{12}$  dsDNA. (a) (Top) Experimental chiral SFG spectra of dsDNA prepared in H<sub>2</sub>O (red) and H<sub>2</sub><sup>18</sup>O (blue) obtained in the N–H/O–H stretching region with the *psp* polarization. Solid black lines are the fit to Eq. (2) (see Methods). (Bottom) Gas-phase density functional theory (DFT) calculation of chiral SFG spectrum of dsDNA shows adenine NH<sub>a</sub>H<sub>b</sub> symmetric (3207  $\text{cm}^{-1}$ ) and asymmetric (3326/3332  $\text{cm}^{-1}$ ) stretching [see Fig. 1(b) for atom labels]. Note that vibrational modes due to water are not included in these DFT calculations. Calculated spectral frequencies were scaled by a factor of 0.95. Chiral SFG response from various orientations of the dsDNA relative to the plane of incidence all show chiral SFG signals of N–H stretching (see Methods and the supplementary material); the selected spectrum shown is for the Euler angles  $\theta = 20^\circ$ ,  $\psi = 150^\circ$ , and averaged around  $\varphi$ . (b) (b-i) Global fits (black) and residuals (yellow) of experimental chiral SFG spectra of dsDNA in H<sub>2</sub>O (red) and H<sub>2</sub><sup>18</sup>O (blue). (b-ii) Fits for C–H and N–H vibrational resonances of dsDNA. (b-iii) Fits for pairs of O–H vibrational resonances of water. The averaged symmetric and asymmetric stretching frequencies are shown, which indicate red-shifts due to the isotopic H<sub>2</sub><sup>18</sup>O substitution, suggesting contributions of water O–H stretching modes to the chiral SFG spectra. a.u.: arbitrary units.

distinguished by H<sub>2</sub><sup>18</sup>O isotopic substitution. Substitution with H<sub>2</sub><sup>18</sup>O is expected to red-shift vibrational bands of the O–H stretching modes of water by  $\sim 12 \text{ cm}^{-1}$ .<sup>19,20,35</sup> Vibrational resonances due to dsDNA should not red-shift.

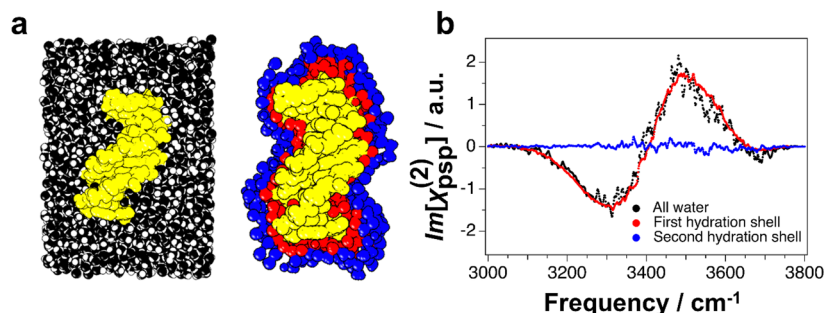
Experimental chiral SFG spectra of dsDNA prepared in H<sub>2</sub>O or H<sub>2</sub><sup>18</sup>O are shown in Fig. 2(a) (top panel). Global fitting of the experimental data [Fig. 2(b) and Table S1] suggests that fitting the experimental spectra requires a minimum of five vibrational resonances of the C–H and N–H stretching of the dsDNA [Fig. 2(b-ii)] and two pairs of hydration water stretching<sup>33</sup> [Fig. 2(b-iii)]. The residual analyses are shown in yellow in Fig. 2(b) (top). Based on the vibrational frequencies, 2966 and 2998  $\text{cm}^{-1}$ , two vibrational resonances are assigned to C–H stretching modes of dsDNA [Fig. 2(b-ii), green curves]. Three vibrational bands in the experimental chiral SFG spectra at 3220, 3357, and 3401  $\text{cm}^{-1}$  [Fig. 2(b-ii), black curves] have not previously been assigned. To assign these vibrational bands, we performed gas-phase calculations of an ideal  $(dA)_{12} \cdot (dT)_{12}$  dsDNA using an exciton model (see Methods and the supplementary material). The calculations [Fig. 2(a), bottom] predict the vibrational resonance at 3207  $\text{cm}^{-1}$  is the symmetric stretching of adenine NH<sub>a</sub>H<sub>b</sub>, while the negative feature at 3326  $\text{cm}^{-1}$  and the positive feature at 3332  $\text{cm}^{-1}$  are attributed to different linear combinations of asymmetric stretching of adenine NH<sub>a</sub>H<sub>b</sub> groups along the dsDNA. Therefore, we propose the vibrational band at 3220  $\text{cm}^{-1}$  in the experimental chiral SFG spectrum is symmetric stretching of adenine NH<sub>a</sub>H<sub>b</sub>, while the vibrational bands at 3357 and 3401  $\text{cm}^{-1}$  are

asymmetric stretching modes of adenine NH<sub>a</sub>H<sub>b</sub> [Fig. 2(b-ii), black curves].<sup>36</sup>

Applying our recently developed theoretical basis for interpreting heterodyne chiral SFG spectra of water,<sup>33</sup> the vibrational resonances of water O–H stretching modes were modeled as pairs of vibrational resonances centered at 3223 and 3503  $\text{cm}^{-1}$  [Fig. 2(b-iii)]. Each pair of vibrations contains two resonances corresponding to symmetric and asymmetric O–H stretching modes of water due to intramolecular coupling. H<sub>2</sub><sup>18</sup>O labeling red-shifts the first pair of vibrational resonances to 3215  $\text{cm}^{-1}$  by 8  $\text{cm}^{-1}$  and red-shifts the second pair to 3466  $\text{cm}^{-1}$  by 37  $\text{cm}^{-1}$ . The magnitude of the red-shift deviates from the expected value of 12  $\text{cm}^{-1}$  likely due to the broad nature of the O–H stretching peak and the uncertainty of the fitting. However, the fitting results capture the red shift induced by the <sup>18</sup>O substitution, supporting water contributions to the chiral SFG spectrum. Because a water molecule is achiral, detection with chiral SFG implies that the hydration structures around dsDNA are chiral.

### Chiral SFG is sensitive to water in the dsDNA first hydration shell

We model the chiral SFG response of water molecules around dsDNA using a dipole-polarizability time correlation function approach with electric field mappings (Fig. 3, see also Methods).<sup>37–41</sup> We built a molecular model of  $(dA)_{12} \cdot (dT)_{12}$  dsDNA using molecular dynamics (MD) in a  $52 \times 52 \times 73 \text{ \AA}^3$  box containing  $\sim 6400$  water molecules and calculated the chiral SFG response of O–H



**FIG. 3.** Chiral SFG response from water molecules surrounding (dA)<sub>12</sub> · (dT)<sub>12</sub> dsDNA in MD simulations. (a) Representative views of the MD simulations including all water molecules (black), and water molecules in the first hydration shell (red) and the second hydration shell (blue) of (dA)<sub>12</sub> · (dT)<sub>12</sub> dsDNA (yellow). (b) Simulated chiral SFG spectra of all water (black), the first hydration shell (red), and the second hydration shell (blue). The first hydration shell (red) shows signals comparable to the total chiral SFG signals (black). The second hydration shell (blue) shows almost no calculated O–H stretching response (right). Vibrational modes due to dsDNA are not included in these calculations. a.u.: arbitrary units.

stretching for all water molecules [Fig. 3(b), black curve]. This calculated chiral SFG response of water spans the spectral region of  $\sim 3100$  to  $3750$   $\text{cm}^{-1}$  and supports our experimental observation of a redshift upon  $\text{H}_2^{18}\text{O}$  substitution of vibrational features in this region [Fig. 2(b-iii)]. We also used the algorithm of Voronoi tessellation<sup>32,42,43</sup> (see Methods and the [supplementary material](#)) to identify water molecules in the first and second hydration shells around dsDNA. Only water molecules in the first hydration shell around dsDNA produce a chiral SFG response [Fig. 3(b), red curve]. Remarkably, water molecules in the second hydration shell around dsDNA produce no chiral SFG response [Fig. 3(b), blue curve]. Thus, both experiment and computation confirm that chiral SFG is sensitive to the O–H stretching modes of water molecules within the first hydration shell around dsDNA and the N–H stretching modes of adenine in (dA)<sub>12</sub> · (dT)<sub>12</sub> dsDNA.

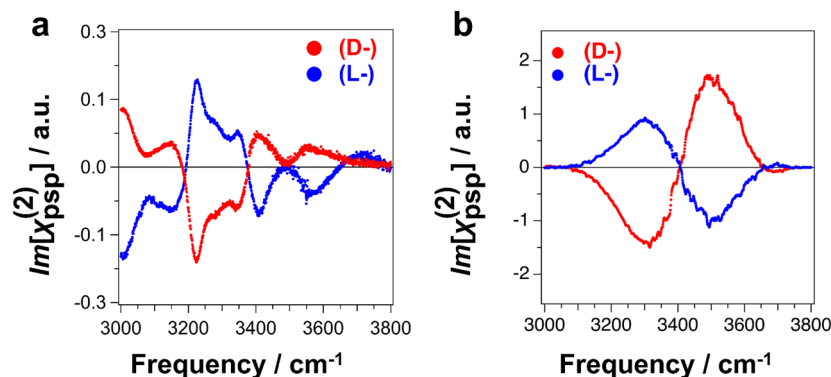
### Chiral SFG detects chirality transfer from dsDNA to water

Heterodyne chiral SFG is sensitive to the macroscopic chirality of the dsDNA double helix.<sup>28</sup> It effectively distinguishes between

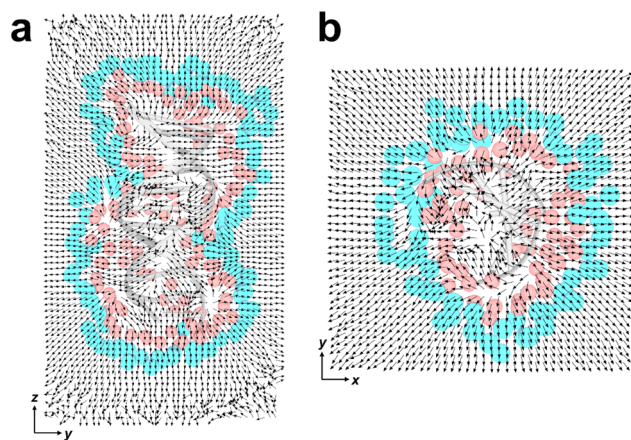
native (D-) and non-native (L-) dsDNA. The chiral SFG spectra of these two enantiomers appear as mirror images of each other with opposite phase [Fig. 4(a)]. Consequently, not only do dsDNA vibrational resonances change phase but also the features assigned above to the O–H stretching of water molecules reverse phase [Fig. 4(a)]. The chiral SFG response of water in the first hydration shell around (D-) or (L-) dsDNA is also calculated to have opposite phase [Fig. 4(b)]. Because the phase from the O–H stretching of water molecules flips with the chirality of the dsDNA, these results imply that the first hydration shell structures around (D-) and (L-) dsDNA possess opposite chirality. Thus, we have identified the origin of the chiral SFG signal of water, namely, chiral hydration structures templated by dsDNA. Furthermore, our experimental and computational results (Fig. 4) establish that chiral SFG detects chirality transfer from dsDNA to the first hydration shell.

### dsDNA chirality transfer to water does not propagate beyond the first hydration shell

What is the origin of chiral SFG selectivity to the dsDNA first hydration shell? Water dipole orientation analysis<sup>32</sup> utilizing a



**FIG. 4.** Native (D-) (dA)<sub>12</sub> · (dT)<sub>12</sub> dsDNA vs non-native (L-) (dA)<sub>12</sub> · (dT)<sub>12</sub> dsDNA and their hydration give mirror-image spectra confirming chirality transfer from dsDNA to hydration water. (a) Experimental chiral SFG spectra of (D-) vs (L-) dsDNA obtained in the C–H/N–H/O–H stretching region with the *psp* polarization. (b) The O–H stretching response of water molecules in the first hydration shell calculated from an MD simulation of (D-) and (L-) dsDNA. Vibrational modes due to dsDNA are not included in these calculations. a.u.: arbitrary units.

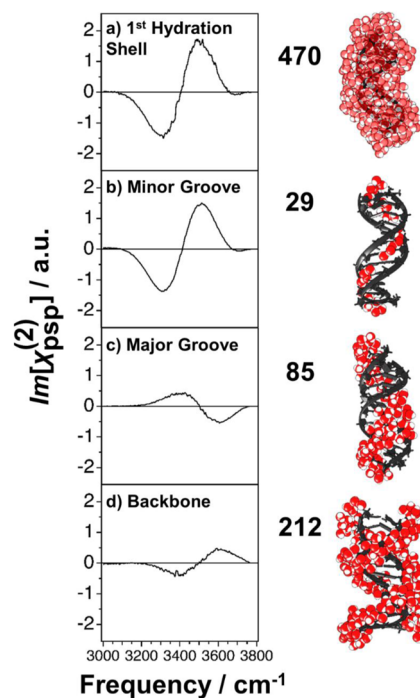


**FIG. 5.** Mean water dipole orientations around  $(dA)_{12} \cdot (dT)_{12}$  dsDNA plotted every 1 Å, averaged over  $1 \times 10^6$  frames of MD simulation. Arrows point toward the water oxygen and bisect the H–O–H angle. Representative structures for the dsDNA and the first (red) and second (blue) hydration shells are guides to the eye. The system was translated to place the DNA's centroid at the origin and rotated as described in the Methods section. (a) Normalized water dipoles projected onto the  $yz$ -plane for water molecules observed with  $0.5 \text{ \AA} \geq x \geq -0.5 \text{ \AA}$ . Note that the  $z = 0 \text{ \AA}$  axis crosses the sixth base pair counting from the top of the DNA structure. (b) Normalized water dipoles projected onto the  $xy$ -plane for water molecules observed with  $0.5 \text{ \AA} \geq z \geq -0.5 \text{ \AA}$ . The section of dsDNA structure shown corresponds to  $10 \text{ \AA} \geq z \geq -10 \text{ \AA}$ .

1 Å-resolution grid reveals that dsDNA creates complex chiral asymmetries in the water population in the first hydration shell (Fig. 5). Furthermore, water molecules in the dsDNA second hydration shell and  $\sim 10$ – $15$  Å beyond the first hydration layer are ordered mostly through interactions with the negative charges on the DNA backbone. However, they exhibit achiral  $C_{\infty v}$  symmetry. Hence, they can possibly generate a conventional (achiral) SFG response via the  $\chi^{(3)}$  contributions,<sup>44–48</sup> but their  $C_{\infty v}$  symmetry is forbidden from generating a chiral SFG response.<sup>25,29–31</sup> Our analysis in Fig. 5 supports the model that chirality transfer from dsDNA to water does not propagate beyond the first hydration shell, whereas water molecules beyond the dsDNA first hydration shell are ordered by the electric field of the negatively-charged phosphate backbone. This model explains our observations (Figs. 3 and 4) that chiral SFG is exclusively sensitive to water molecules in the first hydration shell of dsDNA.

### Chiral SFG can sense chiral hydration structures around dsDNA beyond the “spine of hydration”

To understand which subpopulations of water molecules within the first hydration shell of dsDNA contribute to the chiral SFG response, we calculated the chiral SFG spectra of different subpopulations [Figs. 6(a)–6(d)]. We define these subpopulations using Voronoi analysis (see Methods).<sup>42</sup> Figure 6 shows the chiral SFG spectra of the first hydration shell, including water molecules in the minor and major grooves, and water molecules hydrating the dsDNA backbone. The average number of water molecules in each subpopulation is indicated beside the molecular models.



**FIG. 6.** Calculation of the phase-sensitive chiral SFG response of the O–H stretching modes of water around  $(dA)_{12} \cdot (dT)_{12}$  dsDNA corresponding to water molecules (a) in the first hydration shell, (b) along the minor groove, (c) along the major groove, and (d) along the backbone of dsDNA. All spectra are averaged over  $1 \times 10^6$  frames from 100 ns of MD simulation. Spectral intensities can be directly compared. Note that vibrational modes due to dsDNA are not included in these calculations. The average number of water molecules per MD frame in each subset is listed. Voronoi selection<sup>42</sup> (see Methods) was used to identify water molecule populations around each region of the dsDNA. a.u.: arbitrary units.

The total chiral SFG response of the first hydration shell [Fig. 6(a)] is the sum of the spectral contributions of the subpopulations of water molecules hydrating the minor groove, major groove, and backbone [Figs. 6(b)–6(d)]. Comparison of the absolute intensities of the spectra in Figs. 6(a) and 6(b) shows that the O–H stretching response of water molecules in the dsDNA minor groove accounts for almost the entire chiral SFG response of the first hydration shell. This observation agrees with the proposed molecular origin of water signals surrounding dsDNA.<sup>6</sup> However, to our surprise, the simulated chiral SFG responses of water molecules hydrating the major groove [Fig. 6(c)] and the backbone [Fig. 6(d)] are non-zero but have nearly equal intensity and opposite phase. Thus, the sum of the spectral responses of water hydrating the major groove and backbone is nearly zero due to cancellation (Fig. S2). This result reveals that not only water molecules hydrating the minor groove [Fig. 6(b)] but also those hydrating the major groove and dsDNA backbone [Figs. 6(c) and 6(d)] can contribute to the chiral SFG response [Fig. 6(a)]. This finding implies that chiral SFG can also be used to probe hydration structures of the major groove and backbone of dsDNA. Our result enhances the current understanding of the molecular origins of chiral SFG signals of

water molecules hydrating dsDNA molecules. Notably, experimental chiral SFG methods alone cannot differentiate water molecules hydrating various parts of dsDNA. However, experiments combined with our computational approaches show the promise of chiral SFG for distinguishing different modes of small-molecule binding to dsDNA by detecting displacement of water molecules hydrating the major groove, minor groove, or backbone.

## DISCUSSION

Petersen and co-workers reported the chiral SFG response of  $(dAdT)_{12} \cdot (dAdT)_{12}$  dsDNA in the region  $2600\text{--}3700\text{ cm}^{-1}$  and attributed the observed chiral SFG signal to water molecules embedded in the minor groove of dsDNA.<sup>6</sup> However, our  $H_2^{18}O$  substitution experiment (Fig. 2) and computational investigations (Figs. 2–6) indicate that chiral SFG can detect the O–H stretching of chiral water assemblies around  $(dA)_{12} \cdot (dT)_{12}$  dsDNA, as well as the symmetric stretching ( $3220\text{ cm}^{-1}$ ) and asymmetric stretching ( $3357$  and  $3401\text{ cm}^{-1}$ ) modes of adenine  $NH_aH_b$  (Fig. 2). We also detected chiral SFG response of C–H stretching modes of dsDNA [Fig. 2(b-ii)]. These various modes provide information about the local chemical environments and molecular structures of dsDNA.<sup>28</sup> Our gas-phase calculations of the chiral SFG response of  $(dAdT)_{12} \cdot (dAdT)_{12}$  dsDNA (Fig. S3) suggest that  $NH_aH_b$  stretching resonances are likely to have been convoluted with the O–H stretching of chiral water structures in the previously reported spectra.<sup>6</sup>

Our experimental and computational results reveal that dsDNA transfers chirality to the first hydration shell only (Figs. 3–5). However, a loosely bound hydration shell may extend as far as  $18\text{ \AA}$  from the dsDNA surface due to the electric field of the negatively-charged phosphate backbone.<sup>11</sup> Our water dipole orientation analysis suggests that, beyond the first hydration shell, the electric field of the dsDNA phosphate backbone orders water in achiral  $C_{\infty v}$  symmetry, which cannot generate chiral SFG response according to Simpson's chiral SFG theory (Fig. 5).<sup>20–22,25,29–33</sup> Our analyses support the conclusion that chiral SFG does not report on water molecules beyond the first hydration layer of dsDNA. Therefore, we have established that chiral SFG offers a highly specific method to probe the structure of the dsDNA first hydration shell.

Dissecting the water signals from the first hydration shell around the  $(dA)_{12} \cdot (dT)_{12}$  dsDNA reveals that not only minor groove water molecules but also water subpopulations hydrating the major groove and dsDNA backbone can contribute to the experimental chiral SFG response [Figs. 6(a)–6(d)]. However, the opposite phases and nearly equal intensities of the chiral SFG responses predicted for major groove and backbone waters [Figs. 6(c) and 6(d)] suggest that these signals can destructively interfere and cancel (Fig. S2). Nonetheless, our computational findings revise the notion that the experimental chiral SFG response is only due to water molecules in the dsDNA minor groove.<sup>6,18</sup> For nucleic acid duplexes with different secondary structures (for example, A-DNA or A-RNA, Z-DNA or Z-RNA, or parallel double helices), the major groove and backbone water subpopulations might even dominate the chiral SFG response over minor groove water molecules. Alternatively, the binding of proteins or other molecules to dsDNA may perturb chiral hydration structures. In such cases, the chiral SFG response of water hydrating the major groove and backbone can potentially report

on molecular binding. Our work will guide further development of chiral SFG for studying molecular interactions of dsDNA.

Dickerson and co-workers originally observed the chiral “spine of hydration” in the dsDNA minor groove over 40 years ago.<sup>2,3</sup> As discussed above, however, the chiral SFG response implies the existence of other chiral first hydration shell structures. The spine of hydration can now be interpreted as just one stable chiral hydration structure around dsDNA, alongside the chiral structures formed by major groove and backbone water molecules. Our findings offer an updated scientific perspective in line with recent computational work that has focused on a holistic understanding of hydration structures and dynamics around dsDNA.<sup>7,49</sup>

Based on our findings, chiral SFG experiments and computational analyses are now poised to address fundamental questions related to changes in dsDNA hydration structure during reactions, interactions, recognition, and binding with proteins and small molecules. Heterodyne chiral SFG reveals the phase of the water signals as well as dsDNA vibrational modes and can thereby resolve specific functional groups involved in molecular interactions with dsDNA. Our work has built a rigorous theoretical basis for interpreting chiral SFG spectra of dsDNA hydration, introducing new possibilities to use chiral hydration structures as a novel, label-free reporter for molecular binding to dsDNA.

## METHODS

### DNA oligomer preparation

Cartridge-purified single-stranded DNA oligomers with sequences  $(dA)_{12}$  and  $(dT)_{12}$  were purchased from the Keck Oligonucleotide Synthesis Resource at Yale University and used without further purification. For all experiments, solutions of double-stranded DNA oligomers were prepared at  $100\text{ }\mu\text{M}$ , heated in a water bath at  $80\text{ }^\circ\text{C}$  for 10 min, and allowed to cool in the water bath overnight. Solutions were subsequently stored at  $4\text{ }^\circ\text{C}$ .

### Vibrational SFG measurements

Solutions of dsDNA oligomers were prepared in  $H_2O$  or  $H_2^{18}O$  (Sigma-Aldrich, 97 atom %  $^{18}O$ ). For all SFG experiments,  $10\text{ }\mu\text{l}$  was applied to the clean surface of a right-handed z-cut  $\alpha$ -quartz crystal and the solution was dried in a desiccator. To prevent the exchange of  $H_2^{18}O$  with ambient humidity in hydrated dsDNA films, samples were dried in a sealed container with desiccant under a positive pressure nitrogen flow.

Phase-resolved chiral SFG<sup>50–54</sup> was used to probe hydrated dsDNA films at the quartz surface with the *psp* polarization (*p*-polarized sum frequency, *s*-polarized visible, *p*-polarized infrared) using a homebuilt broadband spectrometer. A Ti:Sapphire regenerative amplifier (Astrella F, Coherent, CA) generates 9 W of 800 nm output with a repetition rate of 5 kHz and 100-fs pulse width. The output is split to generate the tunable IR source by pumping an optical parametric amplifier (OPA) (TOPAS-PRIME, Coherent, CA). This OPA is coupled to a non-collinear difference frequency generator (NDFG, Coherent, CA), which generates broadband infrared pulses tunable from 2.4 to 11  $\mu\text{m}$ , corresponding to the range of  $\sim 900\text{--}4000\text{ cm}^{-1}$ . The remainder of the 800 nm amplifier output enters a 4f pulse shaper for a final pulse duration  $<10\text{ ps}$ . The beams are directed to be coincident on the sample

surface spatially and temporally to generate an SFG signal. The temporal overlap is achieved by a delay stage to change the path length of the infrared beam. The SFG signal generated from the sample surface is collected by a collimating lens and focused into a spectrograph before being detected by a cryogenically cooled CCD camera. The infrared source is *p*-polarized upon exiting the NDFG, while the visible and SFG polarizations are selected using a waveplate and a polarizer.

Chiral SFG spectra were collected with the quartz oriented along the *+y* and *-y* axes of the quartz as calibrated in the laboratory frame (see the [supplementary material](#)).<sup>20</sup> Unless noted otherwise, four spectra (5 min each) were acquired along both the *+y* and *-y* axes and normalized by the clean quartz surface. To obtain the purely imaginary component ( $\text{Im}[\chi^{(2)}]$ ) of the vibrational SFG response, the averages of the normalized measurements along the *+y* and *-y* axes were subtracted according to

$$\text{Im}[\chi^{(2)}] = \frac{(I_{+y} - I_{-y})}{4}. \quad (1)$$

The frequency of SFG spectra was calibrated using polystyrene (Buck Scientific; 0.05 mm film). Spikes of signals due to cosmic rays were manually removed.

The spectra were analyzed using Eq. (2) to model the vibrational resonances. The first term in this expression fits the spectral contributions from C–H and N–H stretches of the dsDNA, where  $\omega_{IR}$  is the frequency of the incident infrared beam, and  $\omega_q$ ,  $\Gamma_q$ , and  $A_q$  are the frequency of the vibrational resonance, the damping factor, and the amplitude of the *q*th vibrational mode, respectively,

$$\text{Im}[\chi^{(2)}] \propto \left[ \sum_q \frac{A_q}{(\omega_{IR} - \omega_q - i\Gamma_q)} + \sum_n \frac{A_n}{(\omega_{IR} - (\omega_n - \frac{1}{2}\Delta\nu) - i\Gamma_n)} - \frac{A_n}{(\omega_{IR} - (\omega_n + \frac{1}{2}\Delta\nu) - i\Gamma_n)} \right]. \quad (2)$$

The second term in Eq. (2) is used to fit the O–H stretching modes. In our previous report,<sup>33</sup> we demonstrated that the chiral SFG responses from water result from intramolecular coupling, causing the symmetric and asymmetric stretching modes of water to appear as two non-degenerate Lorentzian peaks with opposite phase, equal magnitude, and displaced frequency. This term fits the *n*th pair of the symmetric and asymmetric O–H stretching modes of water using shared parameters for amplitude ( $A_n$ ) and width ( $\Gamma_n$ ). The peak positions for both symmetric and asymmetric stretching modes are defined using two parameters, the resonant frequency ( $\omega_n$ ) and the frequency difference ( $\Delta\nu$ ) between the symmetric and asymmetric stretching modes.

Equation (2) was used to globally fit spectra of dsDNA in H<sub>2</sub>O and H<sub>2</sub><sup>18</sup>O, where the peak positions and widths for all N–H and C–H stretching modes were linked, and the width and frequency differences for all pairs of O–H stretching modes were linked. The value of  $\Delta\nu$  was constrained to be between 30 and 150 cm<sup>-1</sup> based on previous studies.<sup>33</sup>

The fitting model used in this work is guided by our previous report,<sup>33</sup> which found that the chiral SFG response of a water O–H stretching band can be described by an “up–down” or “down–up” (doublet) lineshape due to the C<sub>2v</sub> symmetry of a water molecule. A similar lineshape was observed for coupled C=O

oscillators in dsDNA when using vibrational circular dichroism by the Zanni group.<sup>55</sup> Despite the local C<sub>2v</sub> symmetry of the NH<sub>a</sub>H<sub>b</sub> group on adenine (see Fig. 1 for atom labeling), the N–H symmetric and asymmetric stretches need not fit with the doublet model. Greve *et al.*<sup>56</sup> showed significant vibrational coupling between the N3–H<sub>c</sub> and NH<sub>2</sub> modes that removes the local mode symmetry. They found adding this coupling and Fermi resonance with the C6–NH<sub>2</sub> bending mode to be necessary to replicate experimental spectra. Furthermore, any coupling from stacking base pairs would further remove the C<sub>2v</sub> local symmetry. Finally, the NH<sub>2</sub> is bonded to an aromatic system in the nucleobase. The doublet fitting model for chiral SFG response of water was derived<sup>33</sup> based on the individual bond polarizabilities having only diagonal terms ( $\alpha_{aa}$ ,  $\alpha_{bb}$ , and  $\alpha_{cc}$ ) and the resulting molecular hyperpolarizability containing only the effects of the rotated C<sub>∞</sub> bonds. An aromatic system conjugated with the chromophore will likely contribute to the Raman tensor of the system within the plane of conjugation; this means that the system's  $\beta$  (hyperpolarizability) cannot be well represented as the sum of individual bonds, disrupting the model that would produce a doublet.

### Exciton model for simulating N–H stretches of dsDNA

Density functional theory (DFT) calculations were performed on AT Watson–Crick base pairs using the  $\omega$ B97XD functional<sup>57</sup> and the cc-pvdz basis set<sup>58</sup> using Gaussian 16, Rev. C01.<sup>59</sup> A partially solvated model including an explicit water molecule was used to account for the solvation of the NH<sub>2</sub> group on the adenine<sup>60,61</sup> (see Fig. S4). Harmonic analyses were performed to compute normal modes, frequencies, transition dipole moments, and transition Raman polarizability tensors for spectroscopic characterization. See the [supplementary material](#) for additional details.

To account for coupling between different AT base pairs in the SFG spectra, we model the (dA)<sub>12</sub> · (dT)<sub>12</sub> dsDNA using a coupled exciton Hamiltonian of the form<sup>62,63</sup>

$$H = \sum_{j=1}^n \sum_{m_j} \hbar\omega_{m_j} a_{m_j}^+ a_{m_j} + \sum_{j=1}^n \sum_{k>j} \sum_{m_j} \sum_{m_k} \hbar J_{m_j m_k} a_{m_j}^+ a_{m_k} + c.c., \quad (3)$$

where *n* is the total number of base pairs,  $\omega_{m_j}$  represents the *m<sub>j</sub>*th local mode frequency in the *j*th base pair,  $J_{m_j m_k}$  represents the inter-strand vibrational coupling between the *m<sub>j</sub>*th and *m<sub>k</sub>*th vibrational modes in the *j*th and *k*th base pair, and  $a_{m_j}^+$  and  $a_{m_j}$  are creation and annihilation operators of the *m<sub>j</sub>*th mode. In our model, local mode bases are chosen as the normal modes of a single AT Watson–Crick base pair. Local mode frequencies and coupling parameters were determined using the Hessian matrix reconstruction method,<sup>64–66</sup> where only interactions between the first- and second-neighbor base pairs were considered. Simulation and parameterization details are provided in the [supplementary material](#). The exciton model contains the correct physical ingredients and provides physical insight into the origins of the chiral SFG N–H stretching signal; however, it is worth remarking on its limitations. Specifically, the parametrization of the model is performed on an ideal B-DNA structure. As such, the model does not account for conformational fluctuations of the base pairs that might affect the vibrational frequencies and couplings between the vibrational modes.<sup>64</sup> In principle, it is possible to partially account for structural deformations in the model, for example,



by adding diagonal disorder sampled from a Gaussian distribution (inhomogeneous limit).<sup>62</sup> However, based on the symmetry-based chiral SFG theory,<sup>29–31</sup> these fluctuations are not important to confirm spectral contributions of DNA's N–H stretches to the chiral SFG spectra.

Our approach for simulating SFG spectra has been previously described.<sup>26,57–69</sup> Here, we provide only a brief summary. The calculation involves the determination of the second-order molecular hyperpolarizabilities  $\beta_{ijk,q}^{(2)} = \alpha_{ij,q}\mu_{k,q}$ , where  $\alpha_{ij,q}$  and  $\mu_{k,q}$  (with  $i, j, k = x, y, z$ ) are elements of the transition polarizability and dipole moment of the  $q$ th exciton in the molecular frame, respectively. The hyperpolarizability  $\beta_{ijk,q}^{(2)}$  is then rotated to the laboratory frame ( $I, J, K = X, Y, Z$ ) and averaged over the azimuthal angle  $\phi$  in  $5^\circ$  increments to obtain the second-order susceptibility  $\chi_{IJK,q}^{(2)} = \sum_{ijk} \langle R_{Ii}R_{Jj}R_{Kk} \rangle \beta_{ijk,q}^{(2)}$ , where  $R_{Ii}$  represent elements of the  $ZYX$  Euler rotation matrix.<sup>25</sup> The heterodyne SFG spectrum is computed as

$$\text{Im}[\chi^{(2)}](\omega_{IR}) = \text{Im} \sum_q \frac{\chi_{psp,q}^{(2)}}{\omega_{IR} - \omega_q + i\Gamma_q}, \quad (4)$$

where  $\omega_q$  is the frequency of the  $q$ th exciton vibrational mode and the effective  $psp$  susceptibilities are given by<sup>25</sup>

$$\chi_{psp,q}^{(2)} = L_{ZYX}\chi_{ZYX,q}^{(2)} - L_{XYZ}\chi_{XYZ,q}^{(2)}, \quad (5)$$

where  $L_{ijk}$  are Fresnel factors that depend on the refractive index of the interface as well as the incident angle of the lasers.<sup>70,71</sup> The Fresnel factors used in this study are listed in Table S3. The harmonic frequencies were scaled by 0.95, and  $\Gamma_q$  was set to  $4.0 \text{ cm}^{-1}$  to facilitate comparisons with experiments.

### Molecular dynamics simulations

The AMBER tool<sup>72</sup> Nucleic Acid Builder was used to build a  $(dA)_{12} \cdot (dT)_{12}$  B-DNA molecule. The AMBER tool *tleap* was used to solvate and neutralize the system with TIP4P-Ew water<sup>73</sup> and sodium ions, leaving at least  $15 \text{ \AA}$  of solvent on all sides of the dsDNA. The system was then minimized with restraints on the dsDNA [force constant of  $200 \text{ (kcal/mol)/\AA}^2$ ]. This was followed by 500 ps of solvent equilibration with restraints on the dsDNA [ $200 \text{ (kcal/mol)/\AA}^2$ ]. Then, the system was minimized with restraints on the heavy atoms in the dsDNA [ $100 \text{ (kcal/mol)/\AA}^2$ ]. Following this, the system was minimized in three phases with restraints on the dsDNA backbone gradually being released [ $100 \text{ (kcal/mol)/\AA}^2$ , then  $50 \text{ (kcal/mol)/\AA}^2$ , then  $10 \text{ (kcal/mol)/\AA}^2$ ]. This was followed by a minimization of the entire system without restraints. This minimization was followed by 360 ps of temperature annealing in the NPT ensemble (1.013 25 bar, 1 atm) to heat the system from 0 to 300 K. Then, the system was equilibrated in the NPT ensemble for 5 ns, and finally, the system was equilibrated for 5 ns in the NVT ensemble. All energy minimizations used a combination of steepest descent and conjugate gradient approaches. For production runs, the system was propagated for 100 ns in the NVT ensemble, saving conformations every 100 fs. All dynamics used a Langevin integrator with a friction coefficient of 1/picosecond, a temperature of 300 K, and a

timestep of 1 fs. The OL15 force field<sup>74</sup> was used for the dsDNA. The particle–mesh Ewald method<sup>75</sup> was used to calculate long-range electrostatic interactions. Other nonbonded interactions were cut off at  $14 \text{ \AA}$ . Hydrogen-containing bonds within the dsDNA were constrained with the SHAKE algorithm,<sup>76</sup> and the water molecules were kept rigid with the SETTLE method.<sup>77</sup> All minimizations were performed using AMBER pmemd.MPI on 4 CPUs, and all dynamics runs were performed on Nvidia GPUs using CUDA 10.1 and AMBER pmemd.cuda.<sup>72</sup>

### Electric field mapping method for simulating water O–H stretches

SFG spectra were calculated as described previously using Skinner's electric field mapping method<sup>38,40,41</sup> and the inhomogeneous (non-time-dependent) limit approximation to the time-correlation function. Only water molecules in a selected subset (see below) were represented in the exciton Hamiltonian, but all atoms in the system contributed to the electric field experienced by each O–H group in the selected subset. Prior to the calculation of dipoles and polarizabilities, the system was rotated so that the sixth thymine's N3–H<sub>c</sub> bond pointed along the  $y$  axis with the hydrogen atom facing in the positive direction. The  $x$  axis faced in the same general direction as thymine O2; any component in the  $y$ -direction was removed to make the vector perpendicular to the  $y$  axis. The  $z$  axis then faced approximately along the dsDNA helix axis. The entire  $\chi^{(2)}$  tensor was calculated to allow for transformation to another coordinate system. The tensor was rotated using the Euler angles  $\phi$ ,  $\theta$ , and  $\psi$  with the  $zyz$  convention. The tensor was averaged over all values of  $\phi$  using 100 subconformations while being rotated to  $\theta = 20^\circ$  to match the conformation used in the *ab initio* calculations. The  $\psi$  angle had a minimal effect on the spectra and was, thus, set to 0. The  $psp$  response was calculated as  $\chi_{zyx}^{(2)} - \chi_{xyz}^{(2)}$ . The vanishing of the quantity  $\chi_{zyz}^{(2)} - \chi_{yxz}^{(2)}$  was monitored to ensure  $C_\infty$  symmetry was approximately achieved by integration over  $\phi$ .<sup>30</sup> Note that, because the orientation of dsDNA relative to the interface in our experiments is unknown, the absolute phases of the calculated water spectra are ambiguous with respect to the experiment. However, the relative phases and amplitudes of the calculated water spectra are directly comparable to the experiment. Accordingly, all calculated spectra of water around  $(dA)_{12} \cdot (dT)_{12}$  dsDNA were multiplied by a factor of  $-1$  to capture the absolute phases observed in experiments.

### Analysis of water dipole orientation

The water dipole orientation analysis was performed using the MD simulation prepared as described in previous sections. The simulation box was divided into a  $40 \times 40 \times 70 \text{ \AA}^3$  grid centered on the origin with  $1 \text{ \AA}$  spacing. For each frame, the entire system was translated to move the dsDNA's centroid to the origin and then rotated. Each water was assigned to the grid cell in which its oxygen was located. The dipole moment vector of all waters within each cell was summed over the frames and then divided by the number of waters to yield a mean molecular dipole vector. The mean molecular dipole vector was calculated from partial positive charge to partial negative charge on each water molecule, and therefore, the arrows point radially outward from the negatively charged dsDNA. For visualization, representative structures for the first and second hydration shells

were selected via Voronoi tessellation (see the section of Selection of water molecule subsets),<sup>42</sup> and the dsDNA geometry was averaged over all frames. Water molecules are depicted as the van der Waals spheres of their oxygen atoms. UCSF Chimera<sup>78</sup> was used to generate the corresponding figures. In Fig. 5(a), a slice of the hydration shells with  $-5 \text{ \AA} \leq x \leq 0 \text{ \AA}$  was taken and is shown as spheres; mean dipole vectors in grid cells centered on  $x = 0 \text{ \AA}$  were projected onto the  $yz$ -plane and normalized. In Fig. 5(b), a slice of the hydration shells with  $-5 \text{ \AA} \leq z \leq 0 \text{ \AA}$  was taken and is shown as spheres; mean dipole vectors in grid cells centered on  $z = 0 \text{ \AA}$  were projected onto the  $xy$ -plane and normalized.

### Selection of water molecule subsets

Water molecules in the first hydration shell were identified using Voronoi tessellation.<sup>42</sup> Voronoi tessellation defines cells for each atom consisting of the points closer to that atom than to any other atom; this allows for the identification of “neighbors” to any group of atoms. Within the set of first hydration shell water molecules, water subpopulations belonging to the dsDNA minor groove, major groove, and backbone were identified as follows:

- Major groove water molecules** were defined as water molecules closer to an atom of the major groove than to any other atom group in dsDNA.
- Minor groove water molecules** were defined as water molecules within  $3.5 \text{ \AA}$  of the H2 atom on adenine.
- Backbone water molecules** were selected in two steps. First, based on distance, all water molecules closer to backbone atoms than to major- or minor-groove atoms were selected. This produced a selection of water molecules (*selection backbone<sub>1</sub>*) along the backbone, as well as some water molecules near, but not inside, the minor groove. In the second step, these water molecules near the minor groove were removed using Voronoi tessellation.<sup>42</sup> From *selection backbone<sub>1</sub>*, Voronoi tessellation was used to identify water molecules that neighbored the subset of minor groove water molecules [defined previously in (b)], as well as water molecules neighboring the neighbors of minor groove water molecules. All these water molecules were removed from *selection backbone<sub>1</sub>*. The remaining water molecules are defined as backbone water molecules. This two-step selection process was to avoid contamination from water molecules inside or proximal to the minor groove.

All atom selections were made using the MDAnalysis library<sup>79</sup> and in-house Python code. The freud library<sup>80</sup> was used to access the Voronoi tessellation code voro++ from Python.<sup>81</sup>

### SUPPLEMENTARY MATERIAL

The following materials are included in the [supplementary material](#) (PDF): Raw experimental chiral SFG spectra of  $(dA)_{12} \cdot (dT)_{12}$  dsDNA prepared in  $H_2O$  and in  $H_2^{18}O$ , fitting parameters for chiral SFG spectra of  $(dA)_{12} \cdot (dT)_{12}$  dsDNA prepared in  $H_2O$  and in  $H_2^{18}O$ , summation of the calculated chiral SFG spectra of water molecules hydrating the backbone and major groove of  $(dA)_{12} \cdot (dT)_{12}$  dsDNA, calculated chiral SFG spectrum of the N–H stretching response of  $(dAdT)_{12} \cdot (dTdA)_{12}$  dsDNA, complete description of density functional theory and exciton model calculations and

parameters, and orientational dependencies of the calculated chiral SFG spectra of the N–H stretching response of  $(dA)_{12} \cdot (dT)_{12}$  dsDNA.

### ACKNOWLEDGMENTS

The authors thank Garth Simpson (Purdue University) and Martin Zanni (University of Wisconsin-Madison) for insightful comments during the preparation of this manuscript. E.A.P. was supported by the NIH (Grant No. 5T32GM008283-31) and a John C. Tully Chemistry Research Fellowship. D.K. was supported by the NIH (Grant No. 5T32GM008283-32). L.V. acknowledged support from NSF (Grant No. CHE-1753207). V.S.B. acknowledged support from the NSF-CCI Center for Quantum Dynamics on Modular Quantum Devices (CQD-MQD) (Grant No. CHE-2124511). S.H.-S. acknowledged support by the National Institutes of Health Grant No. R35 GM139449. E.C.Y.Y. acknowledged the NSF support (Grant No. CHE-1905169). T.S. was supported by the NSF (Grant No. CHE-1905169 to E.C.Y.Y.) and by the NSF MPS-Ascend Postdoctoral Research Fellowship (Grant No. CHE-2402247 to T.S.).

### AUTHOR DECLARATIONS

#### Conflict of Interest

The authors have no conflicts to disclose.

#### Author Contributions

E.A.P. and D.K. contributed equally to this work.

**Ethan A. Perets:** Conceptualization (equal); Data curation (equal); Formal analysis (equal); Investigation (equal); Methodology (equal); Validation (equal); Visualization (equal); Writing – original draft (equal); Writing – review & editing (equal). **Daniel Konstantinovskiy:** Conceptualization (equal); Data curation (equal); Formal analysis (equal); Investigation (equal); Methodology (equal); Project administration (equal); Software (equal); Validation (equal); Visualization (equal); Writing – original draft (equal); Writing – review & editing (equal). **Ty Santiago:** Data curation (equal); Formal analysis (equal); Investigation (equal); Methodology (equal); Validation (equal); Visualization (equal); Writing – review & editing (equal). **Pablo E. Videla:** Conceptualization (equal); Data curation (equal); Formal analysis (equal); Investigation (equal); Methodology (equal); Software (equal); Validation (equal); Visualization (equal); Writing – original draft (equal); Writing – review & editing (equal). **Matthew Tremblay:** Data curation (equal); Formal analysis (equal); Investigation (equal); Methodology (equal); Software (equal); Validation (equal); Visualization (equal); Writing – original draft (equal); Writing – review & editing (equal). **Luis Velarde:** Funding acquisition (equal); Investigation (equal); Methodology (equal); Supervision (equal); Validation (equal); Writing – review & editing (equal). **Victor S. Batista:** Funding acquisition (equal); Investigation (equal); Supervision (equal); Validation (equal); Writing – review & editing (equal). **Sharon Hammes-Schiffer:** Funding acquisition (equal); Investigation (equal); Methodology (equal); Project administration (equal); Resources (equal); Supervision (equal); Validation (equal); Writing – review & editing (equal). **Elsa C. Y. Yan:** Conceptualization (equal); Formal analysis (equal); Funding acquisition

(equal); Investigation (equal); Methodology (equal); Project administration (equal); Resources (equal); Supervision (equal); Validation (equal); Visualization (equal); Writing – original draft (equal); Writing – review & editing (equal).

## DATA AVAILABILITY

The data that support the findings of this study are available within the article and its [supplementary material](#).

## REFERENCES

- J. D. Watson and F. H. Crick, "Molecular structure of nucleic acids: A structure for deoxyribose nucleic acid," *Nature* **171**(4356), 737–738 (1953).
- R. Dickerson, H. Drew, and B. Conner, *Biomolecular Stereodynamics* (Adenine Press, 1981).
- M. L. Kopka, A. V. Fratini, H. R. Drew, and R. E. Dickerson, "Ordered water structure around a B-DNA dodecamer: A quantitative study," *J. Mol. Biol.* **163**(1), 129–146 (1983).
- V. P. Chuprina, "Anomalous structure and properties of poly (dA)-poly(dT). Computer simulation of the polynucleotide structure with the spine of hydration in the minor groove," *Nucleic Acids Res.* **15**(1), 293–311 (1987).
- E. Liepinsh, G. Otting, and K. Wüthrich, "NMR observation of individual molecules of hydration water bound to DNA duplexes: Direct evidence for a spine of hydration water present in aqueous solution," *Nucleic Acids Res.* **20**(24), 6549–6553 (1992).
- M. L. McDermott, H. Vanselow, S. A. Corcelli, and P. B. Petersen, "DNA's chiral spine of hydration," *ACS Cent. Sci.* **3**(7), 708–714 (2017).
- E. Duboué-Dijon, A. C. Fogarty, J. T. Hynes, and D. Laage, "Dynamical disorder in the DNA hydration shell," *J. Am. Chem. Soc.* **138**(24), 7610–7620 (2016).
- N. J. Tao, S. M. Lindsay, and A. Rupprecht, "Structure of DNA hydration shells studied by Raman spectroscopy," *Biopolymers* **28**(5), 1019–1030 (1989).
- P. Perera, M. Wyche, Y. Loethen, and D. Ben-Amotz, "Solute-induced perturbations of solvent-shell molecules observed using multivariate Raman curve resolution," *J. Am. Chem. Soc.* **130**(14), 4576–4577 (2008).
- T. Elsaesser, J. Schauss, A. Kundu, and B. P. Fingerhut, "Phosphate vibrations probe electric fields in hydrated biomolecules: Spectroscopy, dynamics, and interactions," *J. Phys. Chem. B* **125**(15), 3899–3908 (2021).
- A. K. Singh, C. Wen, S. Cheng, and N. Q. Vinh, "Long-range DNA-water interactions," *Biophys. J.* **120**(22), 4966–4979 (2021).
- S. K. Pal, L. Zhao, and A. H. Zewail, "Water at DNA surfaces: Ultrafast dynamics in minor groove recognition," *Proc. Natl. Acad. Sci. U. S. A.* **100**(14), 8113 (2003).
- M. Yang, Ł. Szyz, and T. Elsaesser, "Decelerated water dynamics and vibrational couplings of hydrated DNA mapped by two-dimensional infrared spectroscopy," *J. Phys. Chem. B* **115**(44), 13093–13100 (2011).
- D. Laage, T. Elsaesser, and J. T. Hynes, "Water dynamics in the hydration shells of biomolecules," *Chem. Rev.* **117**(16), 10694–10725 (2017).
- G. W. H. Wurpel, M. Sovago, and M. Bonn, "Sensitive probing of DNA binding to a cationic lipid monolayer," *J. Am. Chem. Soc.* **129**(27), 8420–8421 (2007).
- P. C. Singh, M. Ahmed, S. Nihonyanagi, S. Yamaguchi, and T. Tahara, "DNA-induced reorganization of water at model membrane interfaces investigated by heterodyne-detected vibrational sum frequency generation spectroscopy," *J. Phys. Chem. B* **126**(4), 840–846 (2022).
- N. M. Levinson, E. E. Bolte, C. S. Miller, S. A. Corcelli, and S. G. Boxer, "Phosphate vibrations probe local electric fields and hydration in biomolecules," *J. Am. Chem. Soc.* **133**(34), 13236–13239 (2011).
- E. A. Perets and E. C. Y. Yan, "The H<sub>2</sub>O helix: The chiral water superstructure surrounding DNA," *ACS Cent. Sci.* **3**(7), 683–685 (2017).
- E. A. Perets and E. C. Y. Yan, "Chiral water superstructures around antiparallel  $\beta$ -sheets observed by chiral vibrational sum frequency generation spectroscopy," *J. Phys. Chem. Lett.* **10**(12), 3395–3401 (2019).
- E. A. Perets, D. Konstantinovsky, L. Fu, J. Chen, H.-F. Wang, S. Hammes-Schiffer, and E. C. Y. Yan, "Mirror-image antiparallel  $\beta$ -sheets organize water molecules into superstructures of opposite chirality," *Proc. Natl. Acad. Sci. U. S. A.* **117**(52), 32902 (2020).
- D. Konstantinovsky, E. A. Perets, E. C. Y. Yan, and S. Hammes-Schiffer, "Simulation of the chiral sum frequency generation response of supramolecular structures requires vibrational couplings," *J. Phys. Chem. B* **125**(43), 12072–12081 (2021).
- E. C. Y. Yan, E. A. Perets, D. Konstantinovsky, and S. Hammes-Schiffer, "Detecting interplay of chirality, water, and interfaces for elucidating biological functions," *Acc. Chem. Res.* **56**(12), 1494–1504 (2023).
- J. Wang, X. Chen, M. L. Clarke, and Z. Chen, "Detection of chiral sum frequency generation vibrational spectra of proteins and peptides at interfaces in situ," *Proc. Natl. Acad. Sci. U. S. A.* **102**(14), 4978 (2005).
- Z. Wang, L. Fu, and E. C. Y. Yan, "C–H stretch for probing kinetics of self-assembly into macromolecular chiral structures at interfaces by chiral sum frequency generation spectroscopy," *Langmuir* **29**(12), 4077–4083 (2013).
- E. C. Y. Yan, L. Fu, Z. Wang, and W. Liu, "Biological macromolecules at interfaces probed by chiral vibrational sum frequency generation spectroscopy," *Chem. Rev.* **114**(17), 8471–8498 (2014).
- E. A. Perets, P. E. Videla, E. C. Y. Yan, and V. S. Batista, "Chiral inversion of amino acids in antiparallel  $\beta$ -sheets at interfaces probed by vibrational sum frequency generation spectroscopy," *J. Phys. Chem. B* **123**(27), 5769–5781 (2019).
- G. Y. Stokes, J. M. Gibbs-Davis, F. C. Boman, B. R. Stepp, A. G. Condie, S. T. Nguyen, and F. M. Geiger, "Making 'sense' of DNA," *J. Am. Chem. Soc.* **129**(24), 7492–7493 (2007).
- E. A. Perets, K. B. Olesen, and E. C. Y. Yan, "Chiral sum frequency generation spectroscopy detects double-helix DNA at interfaces," *Langmuir* **38**(18), 5765–5778 (2022).
- G. J. Simpson, "Molecular origins of the remarkable chiral sensitivity of second-order nonlinear optics," *ChemPhysChem* **5**(9), 1301–1310 (2004).
- A. J. Moad and G. J. Simpson, "A unified treatment of selection rules and symmetry relations for sum-frequency and second harmonic spectroscopies," *J. Phys. Chem. B* **108**(11), 3548–3562 (2004).
- G. J. Simpson, *Nonlinear Optical Polarization Analysis in Chemistry and Biology* (Cambridge University Press, 2017).
- D. Konstantinovsky, E. A. Perets, T. Santiago, L. Velarde, S. Hammes-Schiffer, and E. C. Y. Yan, "Detecting the first hydration shell structure around biomolecules at interfaces," *ACS Cent. Sci.* **8**(10), 1404–1414 (2022).
- D. Konstantinovsky, T. Santiago, M. Tremblay, G. J. Simpson, S. Hammes-Schiffer, and E. C. Y. Yan, "Theoretical basis for interpreting heterodyne chirality-selective sum frequency generation spectra of water," *J. Chem. Phys.* **160**(5), 055102 (2024).
- Z. Li, C. N. Weeraman, M. S. Azam, E. Osman, and J. M. Gibbs-Davis, "The thermal reorganization of DNA immobilized at the silica/buffer interface: A vibrational sum frequency generation investigation," *Phys. Chem. Chem. Phys.* **17**(19), 12452–12457 (2015).
- S.-Y. Jung, S.-M. Lim, F. Albertorio, G. Kim, M. C. Gurau, R. D. Yang, M. A. Holden, and P. S. Cremer, "The Vroman effect: A molecular level description of fibrinogen displacement," *J. Am. Chem. Soc.* **125**(42), 12782–12786 (2003).
- M. Yang, Ł. Szyz, and T. Elsaesser, "Femtosecond two-dimensional infrared spectroscopy of adenine-thymine base pairs in DNA oligomers," *J. Phys. Chem. B* **115**(5), 1262–1267 (2011).
- A. Morita and J. T. Hynes, "A theoretical analysis of the sum frequency generation spectrum of the water surface. II. Time-dependent approach," *J. Phys. Chem. B* **106**(3), 673–685 (2002).
- B. M. Auer and J. L. Skinner, "Dynamical effects in line shapes for coupled chromophores: Time-averaging approximation," *J. Chem. Phys.* **127**(10), 104105 (2007).
- B. M. Auer and J. L. Skinner, "IR and Raman spectra of liquid water: Theory and interpretation," *J. Chem. Phys.* **128**(22), 224511 (2008).
- B. M. Auer and J. L. Skinner, "Vibrational sum-frequency spectroscopy of the water liquid/vapor interface," *J. Phys. Chem. B* **113**(13), 4125–4130 (2009).
- P. A. Pieniazek, C. J. Tainter, and J. L. Skinner, "Interpretation of the water surface vibrational sum-frequency spectrum," *J. Chem. Phys.* **135**(4), 044701 (2011).
- D. Konstantinovsky, E. C. Y. Yan, and S. Hammes-Schiffer, "Characterizing interfaces by Voronoi tessellation," *J. Phys. Chem. Lett.* **14**(23), 5260–5266 (2023).

- <sup>43</sup>A. Rosu-Finsen, "Interfacial interpretation," *Nat. Rev. Chem.* **7**(7), 461 (2023).
- <sup>44</sup>Y.-C. Wen, S. Zha, X. Liu, S. Yang, P. Guo, G. Shi, H. Fang, Y. R. Shen, and C. Tian, "Unveiling microscopic structures of charged water interfaces by surface-specific vibrational spectroscopy," *Phys. Rev. Lett.* **116**(1), 016101 (2016).
- <sup>45</sup>S. Pezzotti, D. R. Galimberti, Y. R. Shen, and M.-P. Gaigeot, "Structural definition of the BIL and DL: A new universal methodology to rationalize nonlinear  $\chi^{(2)}(\omega)$  SFG signals at charged interfaces, including  $\chi^{(3)}(\omega)$  contributions," *Phys. Chem. Chem. Phys.* **20**(7), 5190–5199 (2018).
- <sup>46</sup>T. Joutsuka, T. Hirano, M. Sprik, and A. Morita, "Effects of third-order susceptibility in sum frequency generation spectra: A molecular dynamics study in liquid water," *Phys. Chem. Chem. Phys.* **20**(5), 3040–3053 (2018).
- <sup>47</sup>P. E. Ohno, H.-f. Wang, and F. M. Geiger, "Second-order spectral lineshapes from charged interfaces," *Nat. Commun.* **8**(1), 1032 (2017).
- <sup>48</sup>A. M. Darlington, T. A. Jarisz, E. L. DeWalt-Kerian, S. Roy, S. Kim, M. S. Azam, D. K. Hore, and J. M. Gibbs, "Separating the pH-dependent behavior of water in the stern and diffuse layers with varying salt concentration," *J. Phys. Chem. C* **121**(37), 20229–20241 (2017).
- <sup>49</sup>K. E. Furse and S. A. Corcelli, "Effects of an unnatural base pair replacement on the structure and dynamics of DNA and neighboring water and ions," *J. Phys. Chem. B* **114**(30), 9934–9945 (2010).
- <sup>50</sup>Y. R. Shen, "Surface properties probed by second-harmonic and sum-frequency generation," *Nature* **337**(6207), 519–525 (1989).
- <sup>51</sup>N. Ji, V. Ostroverkhov, C.-Y. Chen, and Y.-R. Shen, "Phase-sensitive sum-frequency vibrational spectroscopy and its application to studies of interfacial alkyl chains," *J. Am. Chem. Soc.* **129**(33), 10056–10057 (2007).
- <sup>52</sup>Y. R. Shen, "Phase-sensitive sum-frequency spectroscopy," *Annu. Rev. Phys. Chem.* **64**(1), 129–150 (2013).
- <sup>53</sup>L. Fu, S.-L. Chen, and H.-F. Wang, "Validation of spectra and phase in sub-1 cm<sup>-1</sup> resolution sum-frequency generation vibrational spectroscopy through internal heterodyne phase-resolved measurement," *J. Phys. Chem. B* **120**(8), 1579–1589 (2016).
- <sup>54</sup>S.-L. Chen, L. Fu, W. Gan, and H.-F. Wang, "Homogeneous and inhomogeneous broadenings and the Voigt line shapes in the phase-resolved and intensity sum-frequency generation vibrational spectroscopy," *J. Chem. Phys.* **144**(3), 034704 (2016).
- <sup>55</sup>A. T. Krummel and M. T. Zanni, "Interpreting DNA vibrational circular dichroism spectra using a coupling model from two-dimensional infrared spectroscopy," *J. Phys. Chem. B* **110**(48), 24720–24727 (2006).
- <sup>56</sup>C. Greve, N. K. Preketes, H. Fidler, R. Costard, B. Koeppe, I. A. Heisler, S. Mukamel, F. Temps, E. T. J. Nibbering, and T. Elsaesser, "N–H stretching excitations in adenosine-thymidine base pairs in solution: Pair geometries, infrared line shapes, and ultrafast vibrational dynamics," *J. Phys. Chem. A* **117**(3), 594–606 (2013).
- <sup>57</sup>J.-D. Chai and M. Head-Gordon, "Long-range corrected hybrid density functionals with damped atom–atom dispersion corrections," *Phys. Chem. Chem. Phys.* **10**(44), 6615–6620 (2008).
- <sup>58</sup>T. H. Dunning, Jr., "Gaussian basis sets for use in correlated molecular calculations. I. The atoms boron through neon and hydrogen," *J. Chem. Phys.* **90**(2), 1007–1023 (1989).
- <sup>59</sup>M. J. Frisch, G. W. Trucks, H. B. Schlegel, G. E. Scuseria, M. A. Robb, J. R. Cheeseman, G. Scalmani, V. Barone, G. A. Petersson, H. Nakatsuji, X. Li, M. Caricato, A. Marenich, J. Bloino, B. G. Janesko, R. Gomperts, B. Mennucci, H. P. Hratchian, J. V. Ortiz, A. F. Izmaylov, J. L. Sonnenberg, D. Williams-Young, F. Ding, F. Lipparini, F. Egidi, J. Goings, B. Peng, A. Petrone, T. Henderson, D. Ranasinghe, V. G. Zakrzewski, J. Gao, N. Rega, G. Zheng, W. Liang, M. Hada, M. Ehara, K. Toyota, R. Fukuda, J. Hasegawa, M. Ishida, T. Nakajima, Y. Honda, O. Kitao, H. Nakai, T. Vreven, K. Throssell, J. A. Montgomery, Jr., J. E. Peralta, F. Ogliaro, M. Bearpark, J. J. Heyd, E. Brothers, K. N. Kudin, V. N. Staroverov, T. Keith, R. Kobayashi, J. Normand, K. Raghavachari, A. Rendell, J. C. Burant, S. S. Iyengar, J. Tomasi, M. Cossi, J. M. Millam, M. Klene, C. Adamo, R. Cammi, J. W. Ochterski, R. L. Martin, K. Morokuma, O. Farkas, J. B. Foresman, and D. J. Fox, Gaussian 16, Revision C.02, Gaussian, Inc., Wallingford, CT, 2016.
- <sup>60</sup>C. S. Peng, K. C. Jones, and A. Tokmakoff, "Anharmonic vibrational modes of nucleic acid bases revealed by 2D IR spectroscopy," *J. Am. Chem. Soc.* **133**(39), 15650–15660 (2011).
- <sup>61</sup>J. J. Ho, D. R. Skoff, A. Ghosh, and M. T. Zanni, "Structural characterization of single-stranded DNA monolayers using two-dimensional sum frequency generation spectroscopy," *J. Phys. Chem. B* **119**(33), 10586–10596 (2015).
- <sup>62</sup>P. Hamm and M. Zanni, *Concepts and Methods of 2D Infrared Spectroscopy* (Cambridge University Press, 2011).
- <sup>63</sup>A. T. Krummel and M. T. Zanni, "DNA vibrational coupling revealed with two-dimensional infrared spectroscopy: Insight into why vibrational spectroscopy is sensitive to DNA structure," *J. Phys. Chem. B* **110**(28), 13991–14000 (2006).
- <sup>64</sup>C. Lee, K.-H. Park, and M. Cho, "Vibrational dynamics of DNA. I. Vibrational basis modes and couplings," *J. Chem. Phys.* **125**(11), 114508 (2006).
- <sup>65</sup>J.-H. Choi and M. Cho, "Computational IR spectroscopy of water: OH stretch frequencies, transition dipoles, and intermolecular vibrational coupling constants," *J. Chem. Phys.* **138**(17), 174108 (2013).
- <sup>66</sup>J.-H. Choi, S. Ham, and M. Cho, "Local amide I mode frequencies and coupling constants in polypeptides," *J. Phys. Chem. B* **107**(34), 9132–9138 (2003).
- <sup>67</sup>M. L. Clark, A. Ge, P. E. Videla, B. Rudshteyn, C. J. Miller, J. Song, V. S. Batista, T. Lian, and C. P. Kubiak, "CO<sub>2</sub> reduction catalysts on gold electrode surfaces influenced by large electric fields," *J. Am. Chem. Soc.* **140**(50), 17643–17655 (2018).
- <sup>68</sup>A. Ge, B. Rudshteyn, P. E. Videla, C. J. Miller, C. P. Kubiak, V. S. Batista, and T. Lian, "Heterogenized molecular catalysts: Vibrational sum-frequency spectroscopic, electrochemical, and theoretical investigations," *Acc. Chem. Res.* **52**(5), 1289–1300 (2019).
- <sup>69</sup>L. Bromley, P. E. Videla, J. L. Cartagena-Brigantty, V. S. Batista, and L. Velarde, "Binding and orientation of carbamate pesticides on silica surfaces," *J. Phys. Chem. C* **127**(17), 8399–8410 (2023).
- <sup>70</sup>H. F. Wang, L. Velarde, W. Gan, and L. Fu, "Quantitative sum-frequency generation vibrational spectroscopy of molecular surfaces and interfaces: Line-shape, polarization, and orientation," *Annu. Rev. Phys. Chem.* **66**, 189–216 (2015).
- <sup>71</sup>X. Zhuang, P. B. Miranda, D. Kim, and Y. R. Shen, "Mapping molecular orientation and conformation at interfaces by surface nonlinear optics," *Phys. Rev. B* **59**(19), 12632–12640 (1999).
- <sup>72</sup>D. A. Case, H. M. Aktulga, K. Belfon, I. Ben-Shalom, S. R. Brozell, D. Cerutti, T. Cheatham III, G. Cisneros, V. Cruzeiro, and T. Darden, Amber 2021, University of California Press, 2021.
- <sup>73</sup>H. W. Horn, W. C. Swope, J. W. Pitera, J. D. Madura, T. J. Dick, G. L. Hura, and T. Head-Gordon, "Development of an improved four-site water model for biomolecular simulations: TIP4P-Ew," *J. Chem. Phys.* **120**(20), 9665–9678 (2004).
- <sup>74</sup>M. Zgarbová, J. Sponer, M. Otyepka, T. E. Cheatham III, R. Galindo-Murillo, and P. J. Jurecka, "Refinement of the sugar–phosphate backbone torsion beta for AMBER force fields improves the description of Z- and B-DNA," *J. Chem. Theory Comput.* **11**(12), 5723–5736 (2015).
- <sup>75</sup>T. Darden, D. York, and L. Pedersen, "Particle mesh Ewald: An  $N \cdot \log(N)$  method for Ewald sums in large systems," *J. Chem. Phys.* **98**(12), 10089–10092 (1993).
- <sup>76</sup>J.-P. Ryckaert, G. Ciccotti, and H. J. Berendsen, "Numerical integration of the cartesian equations of motion of a system with constraints: Molecular dynamics of *n*-alkanes," *J. Comput. Phys.* **23**(3), 327–341 (1977).
- <sup>77</sup>S. Miyamoto and P. A. Kollman, "Settle: An analytical version of the SHAKE and RATTLE algorithm for rigid water models," *J. Comput. Chem.* **13**(8), 952–962 (1992).
- <sup>78</sup>E. F. Pettersen, T. D. Goddard, C. C. Huang, G. S. Couch, D. M. Greenblatt, E. C. Meng, and T. E. Ferrin, "UCSF Chimera—A visualization system for exploratory research and analysis," *J. Comput. Chem.* **25**(13), 1605–1612 (2004).
- <sup>79</sup>N. Michaud-Agrawal, E. J. Denning, T. B. Woolf, and O. Beckstein, "MDAnalysis: A toolkit for the analysis of molecular dynamics simulations," *J. Comput. Chem.* **32**(10), 2319–2327 (2011).
- <sup>80</sup>V. Ramasubramani, B. D. Dice, E. S. Harper, M. P. Spellings, J. A. Anderson, and S. C. Glotzer, "freud: A software suite for high throughput analysis of particle simulation data," *Comput. Phys. Commun.* **254**, 107275 (2020).
- <sup>81</sup>C. Rycroft, "VORO++: A three-dimensional Voronoi cell library in C++," *Chaos* **19**, 041111 (2009).